Research Article Vol. 9, No. 9 / September 2022 / Optica 965

OPTICA

Micro-fabricated mirrors with finesse exceeding one million

Naijun Jin,[1,5] Charles A. McLemore,[2,3] David Mason,[1] James P. Hendrie,[2,3] Yizhi Luo,[1] Megan L. Kelleher,[2,3] Prashanta Kharel,[1] Franklyn Quinlan,[3] Scott A. Diddams,[2,3,4] and Peter T. Rakich[1,6]

[1]Department of Applied Physics, Yale University, New Haven, Connecticut 06520, USA
[2]Department of Physics, University of Colorado Boulder, Boulder, Colorado 80309, USA
[3]National Institute of Standards and Technology, Boulder, Colorado 80305, USA
[4]Department of Electrical, Computer and Energy Engineering, University of Colorado Boulder, Boulder, Colorado 80309, USA
[5]e-mail: naijun.jin@yale.edu
[6]e-mail: peter.rakich@yale.edu

Received 9 June 2022; revised 20 July 2022; accepted 22 July 2022; published 22 August 2022

The Fabry–Perot resonator is one of the most widely used optical devices, enabling scientific and technological breakthroughs in diverse fields including cavity quantum electrodynamics, optical clocks, precision length metrology, and spectroscopy. Though resonator designs vary widely, all high-end applications benefit from mirrors with the lowest loss and highest finesse possible. Fabrication of the highest-finesse mirrors relies on centuries-old mechanical polishing techniques, which offer losses at the parts-per-million (ppm) level. However, no existing fabrication techniques are able to produce high-finesse resonators with the large range of mirror geometries needed for scalable quantum devices and next-generation compact atomic clocks. In this paper, we introduce a scalable approach to fabricate mirrors with ultrahigh finesse ($\geq 10^6$) and user-defined radius of curvature spanning of four orders of magnitude ($10^{-4}-10^{0}$ m). We employ photoresist reflow and reactive ion etching to shape and transfer mirror templates onto a substrate while maintaining sub-Angstrom roughness. This substrate is coated with a dielectric stack and used to create arrays of compact Fabry–Perot resonators with finesse values as high as 1.3 million and measured excess loss <1 ppm. Optical ringdown measurements of 43 devices across five substrates reveal that the fabricated cavity mirrors—with both small and large radii of curvature—produce an average coating-limited finesse of 1.05 million. This versatile approach opens the door to scalable fabrication of high-finesse miniaturized Fabry–Perot cavities needed for emerging quantum optics and frequency metrology technologies.

https://doi.org/10.1364/OPTICA.467440

1. INTRODUCTION

Among optical resonators, high-finesse Fabry–Perot cavities produce unrivaled frequency stability, quality factors, and power handling, enabling scientific and technological breakthroughs in a broad range of applications [1–6]. For the next generation in quantum communications, computation, and timekeeping systems, it will be necessary to bring these performance advantages to compact, integrated platforms [7–9]. This will require a scalable fabrication technique that is flexible enough to meet the varied demands of disparate applications. Many applications benefit from increased finesse, which translates to larger intracavity fields, increased storage times, and narrower linewidths. But geometry can be equally important, as the optimal mode volumes and spot size can vary dramatically for different applications, placing different requirements on the mirror radius of curvature (R). In quantum optics, where the cooperativity between single atoms and optical resonators scales inversely with mode area [10], microcavity geometries with small R ($\sim 10^{-4}-10^{-2}$ m) are desirable. Conversely, for ultra-stable reference cavities in timekeeping applications, frequency noise can be minimized by averaging over thermal fluctuations with large mode areas [11], requiring a large R (~ 1 m).

To maximize finesse ($\mathcal{F}$), it is necessary to minimize all sources of optical loss within the cavity. This is seen from the definition $\mathcal{F}=\pi/(\mathcal{T}+\mathcal{A}+\mathcal{S})$, where $\mathcal{T}$, $\mathcal{A}$, and $\mathcal{S}$ represent the fractional energy loss (per mirror) resulting from transmission, absorption, and scattering, respectively. Thus, an ultrahigh-finesse resonator ($\mathcal{F}>10^6$) requires $\mathcal{T}+\mathcal{A}+\mathcal{S}$ to be at the few ppm level. Using ion-beam sputtering deposition techniques, highly uniform dielectric coatings with absorptive losses ($\mathcal{A}$) of $\sim$1 ppm are available [12]. However, roughness on the mirror surface and subtle imperfections in the mirror shape can both contribute to unwanted scattering losses, resulting in stringent requirements

on the surface quality of the mirror template. For example, at telecom wavelengths, a mirror template with an ideal surface profile (i.e., without any low spatial frequency shape imperfections) must have sub-Angstrom RMS surface roughness to achieve scattering losses ($\mathcal{S}$) below 1 ppm.

Specialized chemical–mechanical polishing techniques, sometimes referred to as super-polishing [13], are used to meet these stringent requirements on individually polished discrete mirror components. This polishing technique can achieve the necessary sub-Angstrom roughness, but only for large-R ($\sim 10\,\text{mm} - 1000\,\text{mm}$) mirrors. Motivated by quantum optics, new fabrication techniques utilizing laser ablation of glass [10,14–17], and chemical etching of silicon [18–21] have been developed in recent years, finding applications in a wide range of experiments [4,22–28]. While these new techniques have the potential for scalable fabrication, they are limited to the production of small-R ($\lesssim$1 mm) mirrors [17,29], with finesse values that fall short of traditional polishing techniques [see comparison in Fig. 1(a)]. Thus, it remains an outstanding challenge to identify a scalable fabrication technique that yields ultrahigh-finesse mirrors, with access to both small and large mode volumes.

In this paper, we demonstrate a wafer-scale fabrication technique that produces ultrahigh-finesse ($\geq 10^6$) mirrors with a user-defined R spanning from 100 μm to 1 m, necessary to satisfy the demanding needs of applications ranging from quantum optics to low-noise laser oscillators. Arrays of microfabricated mirrors are formed on a single substrate using a solvent-vapor based resist reflow process. Through this process, a photoresist defines mirror shapes that are transferred into a substrate using an optimized dry etch, maintaining sub-Angstrom surface roughness. Multilayer mirror coatings are then deposited, creating arrays of compact Fabry–Perot resonators whose performance is evaluated using optical ringdown measurements. Measurements of 43 devices across five substrates (with both small and large R) reveal that the fabricated cavity mirrors produce a mean (maximum) coating-limited finesse of 1.05 million (1.3 million), which, to the best of our knowledge, sets a record among micro-fabricated mirrors (and $R < 10$ mm mirrors in general). This new method thus enables the scalable production of compact Fabry–Perot cavities with the state-of-the-art performance required by emerging technologies.

2. EXPERIMENTAL RESULTS

A. Mirror Fabrication

Through this fabrication approach, we use reflow techniques to create a resist profile that defines the shape of the mirror. Photoresist patterns (MICROPOSIT S1818, positive-tone) are first created on a super-polished substrate (e.g., fused silica) using UV lithography. The single- and multi-level photoresist patterns, seen in Figs. 2(a) and 2(f), are used to form large- and small-R devices, respectively. These resist patterns undergo reflow in a purpose-built solvent-vapor chamber containing propylene glycol methyl ether acetate (PGMEA), a standard solvent for the semiconductor industry; as the photoresist absorbs the solvent vapor, surface tension rounds any sharp corners as it seeks to minimize the surface area of the resist pattern [30]. In the limit of complete reflow, this disk is transformed into a dome [31,32]; however, for intermediate reflow times, a smooth parabolic surface is formed in the center of the resist pattern, as illustrated in Figs. 2(b) and 2(g). An array of 58 such reflowed surfaces formed on a 50 mm wafer is shown in Fig. 1(c). When the photoresist pattern reaches the desired shape, the reflow process is halted, and the resist pattern is transferred into the substrate using an optimized reactive ion etch [33,34], as illustrated in Figs. 2(c), 2(d) and 2(h), 2(i). Note that different etch rates for the photoresist and substrate result in a vertical rescaling of the pattern. After these mirror templates are etched, a multilayer dielectric coating is deposited [Figs. 2(e) and 2(j)], producing an array of concave mirrors.

We achieved control over the reflow by purposely elevating the temperature of the substrate a few degrees higher than the ambient temperature of the solvent vapor. Under this condition, the viscosity of the photoresist can be tuned to permit a relatively fast reflow rate without worry of solvent vapor condensation. Compared with the traditional thermal reflow for making micrometer-scale lenses, this vapor-assisted approach proves to be efficient at making larger structures on the scale of millimeters [30]. Particular attention must be paid to thermalization of the reflow chamber to ensure repeatability and uniformity of the reflow process. Further details and assessment of the fabrication process can be found in Supplement 1 Section S2.

Using this process, one can readily vary the mirror R by four orders of magnitude through control of the initial photoresist

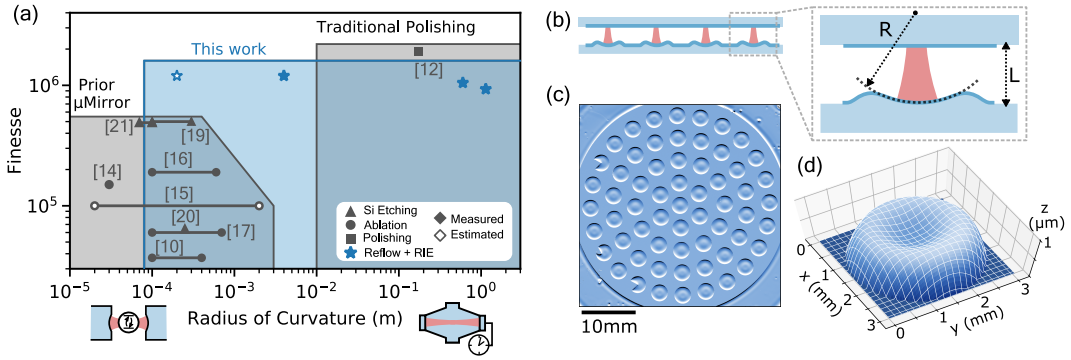

Fig. 1. Micromirror solutions. (a) Survey of micromirror fabrication techniques. The shaded regions and points illustrate the achievable geometry (radius of curvature) and finesse of different techniques. Gray corresponds to prior work including laser ablation (circles), isotropic chemical etching (triangles), and traditional polishing. Blue corresponds to this work. Filled points indicate measured finesses, while unfilled points indicate fabricated mirror templates with finesse predicted based on surface scattering estimates/simulations. Note that these reference finesse values were measured at different optical wavelengths, which will modify the impact of surface scattering. Further details on the literature values are available in Supplement 1 Section S1. (b) Illustration of the cavities built in this work. (c) Image of an array of 58 reflowed photoresist disks on a 50 mm wafer that can be etched to make mirror templates. Non-circular devices on the outer ring are intended for alignment purposes. (d) Measured profile of a fabricated mirror template with $R \approx 1$ m.

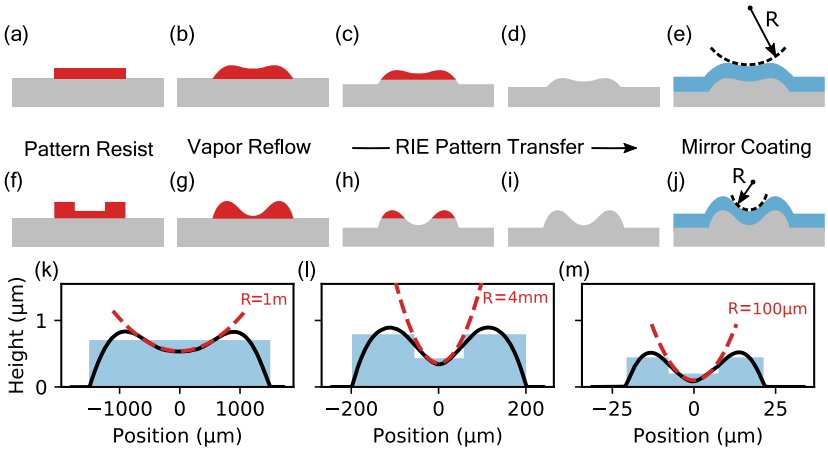

Fig. 2. Micromirror fabrication. The fabrication process begins with a single- (a) or multilayer (f) photoresist pattern. After a timed solvent vapor reflow, a large (b) or small (g) concave photoresist pattern is formed. A reactive ion etch transfers this into the substrate (c), (d), (h), (i), before final application of mirror coating (e), (j). Exemplary measured profiles (black) of reflowed structures with R from 1 m to 100 μm are shown in (k)–(n). Illustrations of the approximate photoresist shape before reflow are shown in blue.

geometry and reflow time. Figures 2(k)–2(m) show measured profiles of etched mirror templates (black) with R ranging from 1 m to 100 μm; approximate resist profiles, used at the beginning of the fabrication process, are illustrated in blue. Note that $R > 1$ m and $R < 100$ μm should be possible with modified photoresist patterns and techniques.

While the measured mirror curvature permits us to leverage Gaussian beam optics as the basis for resonator design, it is important to note that these mirror shapes deviate from a paraboloid at larger radial distances, and the mirrors have a finite size. Thus, in principle, the nontrivial surface profiles produced by the reflow process could contribute to clipping losses, limiting the performance of these mirrors. To investigate limitations posed by these shape-induced losses, we developed a numerical mode solver that builds on the techniques described in Refs. [35,36]. Using a standard (e.g., Hermite–Gaussian) mode basis, this solver encodes a round trip of optical propagation (including the exact mirror profile) into a mode scattering matrix. This scattering matrix is then used to compute the eigenmodes of the resonator, including their associated loss rates. Simulating a plano–concave resonator geometry [Fig. 1(b)] using the measured mirror profile as the input, we find that the shape-induced diffractive losses of optimized mirror templates [Figs. 2(f)–2(j)] are very small (i.e., $\mathcal{S}_{\text{shape}} \leq 0.1$ ppm). In general, this low clipping loss is afforded by relatively deep mirror recesses, which produce large usable apertures. Further details on mirror depth and aperture constraints are available in Supplement 1 Section S2D.

Roughness induced scattering losses are perhaps the most significant barrier to realizing a finesse of greater than 1 million. One can show that the scattering loss associated with an RMS surface roughness, σ_{rms}, is given by $\mathcal{S}_{\text{rough}} = (4\pi\sigma/\lambda)^2$, where λ is the wavelength of light [37]. Hence, at $\lambda = 1550$ nm, each mirror must have sub-Angstrom surface roughness ($\sigma \leq 1.2$ Å) to meet the requirement $\mathcal{S} \leq 1$ ppm. Therefore, the etch process that transfers the photoresist pattern must not appreciably alter the roughness of the super-polished substrate. For this task, we utilize a reactive ion etch that removes material primarily through ion bombardment (i.e., a physical etch) rather than chemical processes (see Supplement 1 Section S2E for further details).

B. Mirror Characterization

The performance of these devices was evaluated by applying a state-of-the-art, ultralow-loss dielectric mirror coating, with alternating SiO_2/Ta_2O_5 layers designed to produce reflectivity >0.99999. We then paired these substrates with flat mirrors from the same coating run, forming arrays of plano–concave Fabry–Perot resonators. These cavities were held in kinematic mounts, or clamped/bonded to an annular spacer. Both small- and large-R mirrors were tested, spanning mode waists from 23 μm to 220 μm. To evaluate the finesse of each resonator, a laser was mode-matched to the fundamental cavity mode, and switched off rapidly after being brought on resonance. Sample transmission ringdowns of small- and large-R cavities are shown in Figs. 3(f) and 3(g). Exponential fits of these measurements reveal cavity lifetimes (τ) of 410 ns and 6.1 μs for small- and large-R resonator devices, corresponding to finesse values of 1.20 million and 1.04 million (using $\mathcal{F} = \pi\tau c/L$, where c is the speed of light, and L is the cavity length), respectively. These lifetime measurements were corroborated using microwave-calibrated frequency sweep measurements. Note that the smallest fabricated devices (with $R \approx 100$ μm) did not receive mirror coatings, but simulations based on their surface profiles predict finesse comparable to the measured devices. Further measurement details are available in Supplement 1 Section S3B.

Ringdown measurements were performed on 43 cavities created using five different patterned micromirror substrates, with results summarized in Figs. 3(b) and 3(c). These measurements indicate consistent performance across the fabricated samples. The small-R cavities all come from a single substrate, containing a grid of 81 micromirrors. Out of 27 mirrors tested, 24 were found to have a finesse >1 million (1.13 ± 0.13 million). The large-R cavities show slightly increased variability (0.91 ± 0.20 million), but still reach a maximum finesse of 1.31 million. This variability is likely due to the increased tilt sensitivity of large-mode-waist cavities, which places more stringent requirements on the mirror symmetry and cavity alignment. We also note that the large-R devices are fabricated on both fused silica and ultralow-expansion (ULE) glass, confirming compatibility with these two technologically important materials [5,6].

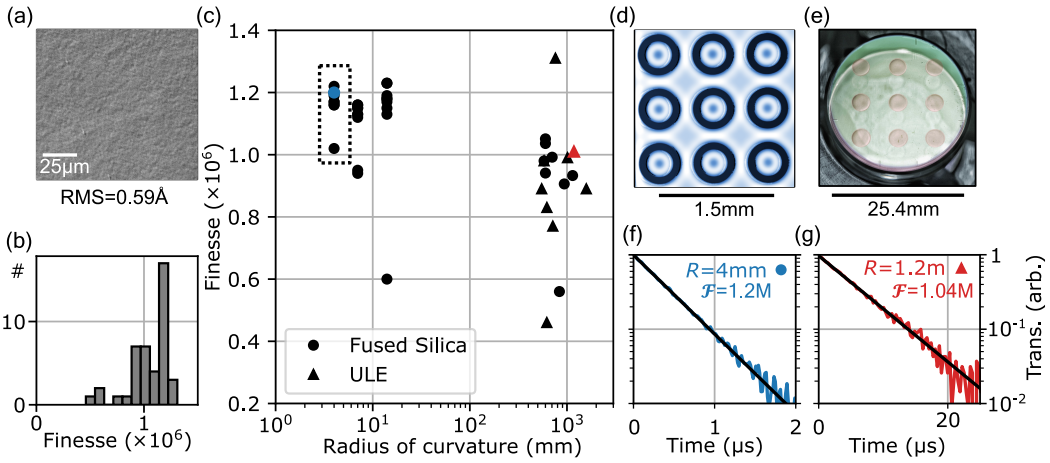

Fig. 3. Mirror characterization and cavity performance evaluation. (a) Dark-field image taken in the center of a large-R ($\approx$1 m) microfabricated mirror, revealing an RMS surface roughness of 0.59 Å. (b), (c) Histogram and summary of cavity finesse measurements for different R micromirrors; 43 cavities, formed on five substrates (both fused silica and ULE) were measured. Exemplary small- and large-R cavities are highlighted in blue and red, respectively, with underlying ringdown data shown in (f) and (g). The dashed box corresponds to the mirror array shown in (d). The nine ULE mirrors are from the substrate shown in (e). (d) Profilometry image of small-R mirror array, corresponding to the dashed box in (c). (e) Image of large-R mirror array on ULE substrate [triangles in (c)]. Mirrors highlighted in false color. (f), (g) Averaged transmission ringdown of a small-R ($R = 4$ mm, $L = 320$ μm) and large-R ($R = 1.2$ m, $L = 5.5$ mm) cavity, where the light is cut off at $t = 0$. Black line is exponential fit yielding 410 ns and 6.1 μs decay time, corresponding to a finesse of 1.20 million and 1.04 million, respectively.

While the finesse permits us to quantify the total mirror loss ($\mathcal{T} + \mathcal{A} + \mathcal{S}$), it is also instructive to separate the different loss contributions. Since both mirrors of all tested microcavities were simultaneously coated, receiving an identical multilayer coating, it is reasonable to assume that the transmission coefficients ($\mathcal{T}$) are identical for both mirrors. With this assumption, we can extract ($\mathcal{A} + \mathcal{S}$) from the relative transmitted and reflected powers on resonance [38]. Doing so, we estimate $\mathcal{T} = 1.9$ ppm for this coating, which means that, for our measured $\mathcal{F} = 1.2 \times 10^6$, we infer the excess loss to be ($\mathcal{A} + \mathcal{S}$) ≈ 0.74 ppm. Note that since these dissipative loss channels are smaller than the external loss ($\mathcal{T}$), this resonator technology offers a path to efficient light extraction at these ultrahigh-finesse levels.

3. OUTLOOK

Building on these techniques, one could envision using wafer-scale fabrication approaches (pictured in Fig. 4) to bring the unique advantages offered by high-finesse Fabry–Perot resonators to integrated systems. In contrast to dielectric waveguide resonators, the modes of Fabry–Perot resonators can be engineered to live almost entirely in vacuum, avoiding problematic sources of thermorefractive noise produced by dielectrics [39,40]. For this reason, ultrahigh-finesse cavities, of the type fabricated in this paper, could prove instrumental to satisfy the growing demand for frequency stabilized ultranarrow-linewidth lasers for atomic clocks, communications, and sensing applications. For such applications, large mode sizes ($\gtrsim$200 μm) produced by larger R ($\gtrsim$1 m) mirrors are used to suppress residual noise generated by the mirror coating. Such frequency-stabilized cavities are typically constructed from ULE glass to eliminate expansion-induced frequency drift. Through a separate study, a bonded cavity assembly, using 1-m-R micromirrors from Fig. 3(c), was shown to produce a thermal-noise-limited fractional frequency instability of 7×10^{-15} at 1 s, in a volume of only 8 mL [41]. This same device was also used to lock an integrated semiconductor laser using the Pound–Drever–Hall (PDH) technique, yielding ~1 Hz integral linewidth on the time scale of a second [42]. Pushing towards even larger R on larger mirrors, one could adopt grayscale lithography to define mirror shapes in the first step and use reflow to make smooth surfaces.

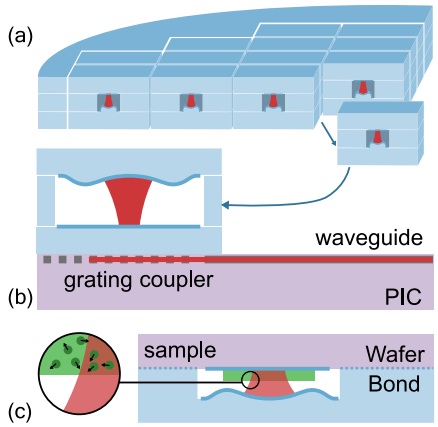

Fig. 4. Integrated microcavity outlook. (a) Illustration of large-scale micro-Fabry–Perot assembly and integration, in which a planar mirror wafer is bonded to a micromachined spacer layer and a micromirror array wafer. (b), (c) Illustration of possible applications: (b) integration of micro-Fabry–Perot with photonic integrated circuit (PIC); (c) bonding of recessed mirrors to form low-volume resonators for cavity QED.

Conversely, small-R mirrors can yield small mode volumes necessary to produce enhanced coupling rates with atoms, ions, and defect centers for quantum applications [22,23,27,28] [see Fig. 4(c)]. For example, the smallest microcavities studied here ($R = 4$ mm, $L = 320$ μm) produce modes with a waist radius of 23 μm and finesse of 1.2 million, corresponding to a Purcell enhancement factor of ~1000 [43], which could already enable strong coupling to quantum emitters. Since the modes of such Gaussian beam resonators are readily mode-matched to optical fibers, they permit highly efficient collection of photons required

for cavity quantum electrodynamics and quantum networking applications.

To harness these and other performance advantages, one could envision integrating such high-finesse resonators with planar photonic circuits using vertical-emission grating couplers [44], as seen in Fig. 4(b). In the context of integrated photonics, these high-finesse resonators are also remarkable for their ability to produce very high Q-factors ($Q > 10$ billion) within compact footprints ($\sim$1 mm^2) Hence, these resonators could offer compelling performance advantages relative to state-of-the-art ring resonators [45,46] and dielectric resonators [47], opening the door to scalable integrated photonic technologies.

Funding. National Institute of Standards and Technology (NOAC); Defense Advanced Research Projects Agency (a-Phi, FA9453-19-C0029); U.S. Department of Energy (DE-SC0019406).

Acknowledgment. Device fabrication was carried out with support from the Yale SEAS Cleanroom and Yale West Campus Cleanroom. We thank Yong Sun, Sean Rinehart, Kelly Woods, Min Li, Lei Wang, Yubo Wang, and Hong X. Tang for their assistance in device fabrication. We thank Lindsay Sonderhouse and Jules Stuart for helpful comments on the manuscript, and Ramin Lalezari of FiveNine Optics for assistance in characterizing mirror surface quality.

Disclosures. Identification of commercial vendors is for scientific clarity only and does not represent endorsement by NIST. The authors declare no conflicts of interest.

Data availability. Data underlying the results presented in this paper are not publicly available at this time but may be obtained from the authors upon reasonable request.

Supplemental document. See Supplement 1 for supporting content.

REFERENCES

1. R. J. Thompson, G. Rempe, and H. J. Kimble, "Observation of normal-mode splitting for an atom in an optical cavity," Phys. Rev. Lett. **68**, 1132–1135 (1992).
2. A. Reiserer and G. Rempe, "Cavity-based quantum networks with single atoms and optical photons," Rev. Mod. Phys. **87**, 1379–1418 (2015).
3. J. McKeever, A. Boca, A. D. Boozer, R. Miller, J. R. Buck, A. Kuzmich, and H. J. Kimble, "Deterministic generation of single photons from one atom trapped in a cavity," Science **303**, 1992–1994 (2004).
4. Y. Colombe, T. Steinmetz, G. Dubois, F. Linke, D. Hunger, and J. Reichel, "Strong atom-field coupling for Bose-Einstein condensates in an optical cavity on a chip," Nature **450**, 272–276 (2007).
5. D. G. Matei, T. Legero, S. Häfner, C. Grebing, R. Weyrich, W. Zhang, L. Sonderhouse, J. M. Robinson, J. Ye, F. Riehle, and U. Sterr, "1.5 μm lasers with sub-10 MHz linewidth," Phys. Rev. Lett. **118**, 263202 (2017).
6. T. M. Fortier, M. S. Kirchner, F. Quinlan, J. Taylor, J. C. Bergquist, T. Rosenband, N. Lemke, A. Ludlow, Y. Jiang, C. W. Oates, and S. A. Diddams, "Generation of ultrastable microwaves via optical frequency division," Nat. Photonics **5**, 425–429 (2011).
7. Z. L. Newman, V. Maurice, T. Drake, J. R. Stone, T. C. Briles, D. T. Spencer, C. Fredrick, Q. Li, D. Westly, B. R. Ilic, B. Shen, M.-G. Suh, K. Y. Yang, C. Johnson, D. M. S. Johnson, L. Hollberg, K. J. Vahala, K. Srinivasan, S. A. Diddams, J. Kitching, S. B. Papp, and M. T. Hummon, "Architecture for the photonic integration of an optical atomic clock," Optica **6**, 680–685 (2019).
8. V. Maurice, Z. L. Newman, S. Dickerson, M. Rivers, J. Hsiao, P. Greene, M. Mescher, J. Kitching, M. T. Hummon, and C. Johnson, "Miniaturized optical frequency reference for next-generation portable optical clocks," Opt. Express **28**, 24708–24720 (2020).
9. D. T. Spencer, T. Drake, T. C. Briles, J. Stone, L. C. Sinclair, C. Fredrick, Q. Li, D. Westly, B. R. Ilic, A. Bluestone, N. Volet, T. Komljenovic, L. Chang, S. H. Lee, D. Y. Oh, M.-G. Suh, K. Y. Yang, M. H. P. Pfeiffer, T. J. Kippenberg, E. Norberg, L. Theogarajan, K. Vahala, N. R. Newbury, K. Srinivasan, J. E. Bowers, S. A. Diddams, and S. B. Papp, "An optical-frequency synthesizer using integrated photonics," Nature **557**, 81–85 (2018).
10. D. Hunger, T. Steinmetz, Y. Colombe, C. Deutsch, T. W. Hänsch, and J. Reichel, "A fiber Fabry-Perot cavity with high finesse," New J. Phys. **12**, 065038 (2010).
11. Y. Levin, "Internal thermal noise in the LIGO test masses: a direct approach," Phys. Rev. D **57**, 659–663 (1998).
12. G. Rempe, R. J. Thompson, H. J. Kimble, and R. Lalezari, "Measurement of ultralow losses in an optical interferometer," Opt. Lett. **17**, 363–365 (1992).
13. J. Nelson and S. Iles, "Creating sub angstrom surfaces on planar and spherical substrates," Proc. SPIE **11175**, 1117505 (2019).
14. A. Muller, E. B. Flagg, J. R. Lawall, and G. S. Solomon, "Ultrahigh-finesse, low-mode-volume Fabry-Perot microcavity," Opt. Lett. **35**, 2293–2295 (2010).
15. D. Hunger, C. Deutsch, R. J. Barbour, R. J. Warburton, and J. Reichel, "Laser micro-fabrication of concave, low-roughness features in silica," AIP Adv. **2**, 012119 (2012).
16. M. Uphoff, M. Brekenfeld, G. Rempe, and S. Ritter, "Frequency splitting of polarization eigenmodes in microscopic Fabry-Pérot cavities," New J. Phys. **17**, 013053 (2015).
17. H. Takahashi, J. Morphew, F. Oručević, A. Noguchi, E. Kassa, and M. Keller, "Novel laser machining of optical fibers for long cavities with low birefringence," Opt. Express **22**, 31317–31328 (2014).
18. M. Trupke, E. A. Hinds, S. Eriksson, E. A. Curtis, Z. Moktadir, E. Kukharenka, and M. Kraft, "Microfabricated high-finesse optical cavity with open access and small volume," Appl. Phys. Lett. **87**, 211106 (2005).
19. G. Wachter, S. Kuhn, S. Minniberger, C. Salter, P. Asenbaum, J. Millen, M. Schneider, J. Schalko, U. Schmid, A. Felgner, D. Hüser, M. Arndt, and M. Trupke, "Silicon microcavity arrays with open access and a finesse of half a million," Light Sci. Appl. **8**, 37 (2019).
20. G. W. Biedermann, F. M. Benito, K. M. Fortier, D. L. Stick, T. K. Loyd, P. D. Schwindt, C. Y. Nakakura, R. L. Jarecki, and M. G. Blain, "Ultrasmooth microfabricated mirrors for quantum information," Appl. Phys. Lett. **97**, 181110 (2010).
21. J. Fait, S. Putz, G. Wachter, J. Schalko, U. Schmid, M. Arndt, and M. Trupke, "High finesse microcavities in the optical telecom O-band," Appl. Phys. Lett. **119**, 221112 (2021).
22. B. Merkel, A. Ulanowski, and A. Reiserer, "Coherent and purcell-enhanced emission from erbium dopants in a cryogenic high-Q resonator," Phys. Rev. X **10**, 041025 (2020).
23. H. Takahashi, E. Kassa, C. Christoforou, and M. Keller, "Strong coupling of a single ion to an optical cavity," Phys. Rev. Lett. **124**, 013602 (2020).
24. M. Steiner, H. M. Meyer, C. Deutsch, J. Reichel, and M. Köhl, "Single ion coupled to an optical fiber cavity," Phys. Rev. Lett. **110**, 043003 (2013).
25. A. D. Kashkanova, A. B. Shkarin, C. D. Brown, N. E. Flowers-Jacobs, L. Childress, S. W. Hoch, L. Hohmann, K. Ott, J. Reichel, and J. G. E. Harris, "Superfluid brillouin optomechanics," Nat. Phys. **13**, 74–79 (2017).
26. N. E. Flowers-Jacobs, S. W. Hoch, J. C. Sankey, A. Kashkanova, A. M. Jayich, C. Deutsch, J. Reichel, and J. G. E. Harris, "Fiber-cavity-based optomechanical device," Appl. Phys. Lett. **101**, 221109 (2012).
27. E. Janitz, M. Ruf, M. Dimock, A. Bourassa, J. Sankey, and L. Childress, "Fabry-Perot microcavity for diamond-based photonics," Phys. Rev. A **92**, 043844 (2015).
28. R. Albrecht, A. Bommer, C. Deutsch, J. Reichel, and C. Becher, "Coupling of a single nitrogen-vacancy center in diamond to a fiber-based microcavity," Phys. Rev. Lett. **110**, 243602 (2013).
29. K. Ott, S. Garcia, R. Kohlhaas, K. Schüppert, P. Rosenbusch, R. Long, and J. Reichel, "Millimeter-long fiber Fabry-Perot cavities," Opt. Express **24**, 9839–9853 (2016).
30. A. Emadi, H. Wu, S. Grabarnik, G. D. Graaf, and R. F. Wolffenbuttel, "Vertically tapered layers for optical applications fabricated using resist reflow," J. Micromech. Microeng. **19**, 074014 (2009).
31. P. Kharel, Y. Chu, M. Power, W. H. Renninger, R. J. Schoelkopf, and P. T. Rakich, "Ultra-high-Q phononic resonators on-chip at cryogenic temperatures," APL Photon. **3**, 066101 (2018).
32. L. Li, T. Abe, and M. Esashi, "Fabrication of miniaturized bi-convex quartz crystal microbalance using reactive ion etching and melting photoresist," Sens. Actuators A, Phys. **114**, 496–500 (2004).
33. L. Li, T. Abe, and M. Esashi, "Smooth surface glass etching by deep reactive ion etching with SF_6 and Xe gases," J. Vac. Sci. Technol. B **21**, 2545–2549 (2003).
34. M. D. Minnick, G. A. Devenyi, and R. N. Kleiman, "Optimum reactive ion etching of x-cut quartz using SF_6 and Ar," J. Micromechan. Microeng. **23**, 117002 (2013).

35. D. Kleckner, W. T. Irvine, S. S. Oemrawsingh, and D. Bouwmeester, "Diffraction-limited high-finesse optical cavities," Phys. Rev. A **81**, 043814 (2010).
36. J. Benedikter, T. Hümmer, M. Mader, B. Schlederer, J. Reichel, T. W. Hänsch, and D. Hunger, "Transverse-mode coupling and diffraction loss in tunable Fabry-Pérot microcavities," New J. Phys. **17**, 053051 (2015).
37. H. Bennett and J. Porteus, "Relation between surface roughness and specular reflectance at normal incidence," J. Opt. Soc. Am. **51**, 123–129 (1961).
38. C. J. Hood, H. J. Kimble, and J. Ye, "Characterization of high-finesse mirrors: loss, phase shifts, and mode structure in an optical cavity," Phys. Rev. A **64**, 033804 (2001).
39. M. L. Gorodetsky and I. S. Grudinin, "Fundamental thermal fluctuations in microspheres," J. Opt. Soc. Am. B **21**, 697–705 (2004).
40. V. Braginsky, M. Gorodetsky, and S. Vyatchanin, "Thermo-refractive noise in gravitational wave antennae," Phys. Lett. A **271**, 303–307 (2000).
41. C. A. McLemore, N. Jin, M. L. Kelleher, J. P. Hendrie, D. Mason, Y. Luo, D. Lee, P. Rakich, S. A. Diddams, and F. Quinlan, "Thermal noise-limited laser stabilization to an 8 mL volume Fabry-Pérot reference cavity with microfabricated mirrors," arXiv:2203.15915 (2022).
42. J. Guo, C. A. McLemore, C. Xiang, D. Lee, L. Qu, W. Jin, M. Kelleher, N. Jin, D. Mason, L. Chang, A. Feshali, M. Paniccia, P. T. Rakich, K. J. Vahala, S. A. Diddams, F. Quinlan, and J. E. Bowers, "Chip-based laser with 1 Hertz integrated linewidth," arXiv:2203.16739 (2022).
43. E. M. Purcell, "Spontaneous emission probabilities at radio frequencies," in *Confined Electrons and Photons: New Physics and Applications*, E. Burstein and C. Weisbuch, eds., NATO ASI series (Springer, 1995), pp. 839.
44. L. Cheng, S. Mao, Z. Li, Y. Han, and H. Fu, "Grating couplers on silicon photonics: design principles, emerging trends and practical issues," Micromachines **11**, 666 (2020).
45. M. W. Puckett, K. Liu, N. Chauhan, Q. Zhao, N. Jin, H. Cheng, J. Wu, R. O. Behunin, P. T. Rakich, K. D. Nelson, and D. J. Blumenthal, "422 million intrinsic quality factor planar integrated all-waveguide resonator with sub-MHz linewidth," Nat. Commun. **12**, 934 (2021).
46. H. Lee, M.-G. Suh, T. Chen, J. Li, S. A. Diddams, and K. J. Vahala, "Spiral resonators for on-chip laser frequency stabilization," Nat. Commun. **4**, 2468 (2013).
47. A. A. Savchenkov, A. B. Matsko, V. S. Ilchenko, and L. Maleki, "Optical resonators with ten million finesse," Opt. Express **15**, 6768–6773 (2007).